IEEE Access
Multidisciplinary | Rapid Review | Open Access Journal

Received September 18, 2019, accepted October 21, 2019, date of publication November 6, 2019,
date of current version November 20, 2019.

Digital Object Identifier 10.1109/ACCESS.2019.2951916

Automatic Electron Density Determination by Using a Convolutional Neural Network

TATSUHITO HASEGAWA[1], (Member, IEEE), SHOYA MATSUDA[2], ATSUSHI KUMAMOTO[3], FUMINORI TSUCHIYA[3], YOSHIYA KASAHARA[4], YOSHIZUMI MIYOSHI[5], (Member, IEEE), YASUMASA KASABA[3], AYAKO MATSUOKA[2], AND IKU SHINOHARA[2]

[1]Graduate School of Engineering, University of Fukui, Fukui 910-8507, Japan
[2]Institute of Space and Astronautical Science, Japan Aerospace Exploration Agency, Sagamihara 252-0203, Japan
[3]Graduate School of Science, Tohoku University, Sendai 980-8578, Japan
[4]Graduate School of Natural Science and Technology, Kanazawa University, Kanazawa 920-1192, Japan
[5]Institute for Space-Earth Environmental Research, Nagoya University, Nagoya 464-8601, Japan

Corresponding author: Tatsuhito Hasegawa (t-hase@u-fukui.ac.jp)

This work was supported in part by the Grants-in-Aid for Scientific Research through the Ministry of Education, Culture, Sports, Science, and Technology in Japan under Grant 14J02108, Grant 17K05668, Grant 15H05815, Grant 16H04056, Grant 16H06286, Grant 17H00728, and Grant 18H04441, and in part by the Japan Society for the Promotion of Science (JSPS) Bilateral Open Partnership Joint Research Projects.

ABSTRACT In this study, we developed a technique for automatically determining upper hybrid resonance (UHR) frequencies using a convolutional neural network (CNN) to derive the electron density along the orbit of the Arase satellite. We used three CNN models (AlexNet, VGG16 and ResNet) to determine the UHR frequencies without additional features based on an expert's knowledge. We also reproduced the multi-layer perceptron (MLP) model that had been used for the Van Allen probes mission, which requires observed electric field spectra and additional five features (i.e., decimal logarithm of electron cyclotron frequency ($\log_{10} f_{ce}$), L-value, geomagnetic index (K_p), magnetic local time, and frequency bin with the highest power spectral density from the electric field spectra ($f\,\mathrm{bin}_{\max}$)). We confirmed that the proposed method using CNN more accurately determined the UHR frequencies than did the conventional method. The mean absolute error (MAE) of the VGG16 model was 3.478 bins when the input vector comprised both the observed electric field spectrum and the additional five features. In contrast, the MAE of the conventional method was 5.986 bins (72.1% worse). Moreover, we confirmed that the proposed method achieves a high accuracy regardless of the use of the additional five features (the MAE of the ResNet model was 3.664 bins when excluding the additional five features). This suggests that the feature map of the ResNet model acquired a representation ability beyond the five features.

INDEX TERMS Computer aided analysis, machine intelligence, magnetosphere, plasma waves.

I. INTRODUCTION

It is well known that ambient electron density is an important property of space plasma. The radial structures of the terrestrial ionosphere and plasmasphere are characterized by variations of ambient electron density. For example, the outer edge of the plasmasphere is called the plasmapause and/or plasmasphere boundary layer and is defined as the location of a sudden decrease in ambient electron density [1], [2]. The location of the plasmapause varies according to geomagnetic conditions and is well correlated with geomagnetic indices (K_p), as demonstrated by Carpenter and Anderson [3]. The evolution of the plasmasphere is important when studying the role of a geomagnetic storm in geospace.

Another important point is that the generation and propagation properties of plasma waves are strongly dependent on in-situ ambient plasma conditions [4]. The knee whistler discovered by Carpenter [1] serves as evidence that the ambient electron density gradient along a magnetic field line can affect the properties of plasma wave propagation. It is also important to note that ambient electron density is a key parameter of wave-particle interactions and plays an important role in the cross-energy coupling process in geospace [5], [6].

Direct measurement of the total ambient plasma density from low energy to high energy is difficult because of spacecraft charging effects. However, the determination of upper hybrid resonance (UHR) frequency is an established method

The associate editor coordinating the review of this manuscript and approving it for publication was Wu-Shiung Feng.

that quantitatively derive ambient electron density. From the measured frequency of the observed UHR emissions (f_{UHR}), we can estimate the electron plasma frequency (f_{p}).

$$f_{\mathrm{UHR}} = \sqrt{f_{\mathrm{p}}^2 + f_{\mathrm{c}}^2}, \tag{1}$$

where f_{c} denotes the local electron cyclotron frequency, which is easily calculated from the in-situ magnetic field measurement. The ambient electron density, n, is then determined by inserting the estimated f_{p} into (2):

$$f_{\mathrm{p}} = \frac{1}{2\pi}\sqrt{\frac{ne^2}{m\epsilon_0}}, \tag{2}$$

where e and m denote the charge and mass of an electron, respectively, and ϵ_0 denotes the permittivity of free space.

The high frequency analyzer (HFA) is a subsystem of the plasma wave experiment (PWE) aboard Arase [7]–[9]. The HFA measures electric field spectra in the frequency range of 10 kHz to 10 MHz, which covers the typical range of UHR frequencies in the inner magnetosphere. The UHR frequencies observed using the PWE/HFA have been utilized in several recent studies. For example, Shinbori *et al.* [10] investigated the temporal and spatial variations of the ionospheric trough during a geomagnetic storm using in-situ electron density calculated from UHR frequencies observed by the PWE/HFA and from the global navigation satellite system total electron content (GNSS-TEC) data. Kotov *et al.* [11] compared the electron density at Arase's altitude and measured the topside ionosphere using the incoherent scatter radar at Kharkiv, Ukraine.

Kumamoto *et al.* [8] proposed a method for the identification of UHR frequencies using a semiautomatic detection algorithm with correction by a human operator via visual inspection. This method is used to determine the UHR frequencies from electric field spectra observed by the PWE/HFA aboard Arase. However, this approach requires enormous effort from the human operator, and two difficulties were reported: the first is that the number of HFA spectrograms is too large for a manual trace of the UHR emissions in the spectrogram; the second is that there are cases wherein UHR emissions are difficult to identify. In addition, as long as the Arase satellite continues its scientific operation, the determination of UHR frequencies from newly observed electric field spectra will have to continue. Because of these drawbacks, an alternative state-of-the-art way of determining UHR frequencies is required.

Kurth *et al.* [12] developed the automated upper hybrid resonance detection algorithm (AURA) to effectively determine UHR frequencies. AURA performs numerical spectrum analysis based on the theory of plasma waves. Kurth et al. applied their algorithm to electric field spectra observed by the Electric and Magnetic Field Instrument Suite and Integrated Science (EMFISIS) equipment aboard the Van Allen probes [13] and achieved an accuracy of up to 10% of the resulting electron density, excluding cases of low density.

Zhelavskaya *et al.* [14] proposed the neural-network-based upper hybrid resonance determination (NURD) algorithm for automatic determination of UHR frequencies observed by EMFISIS, using the local electron cyclotron frequency (f_{ce}), orbital parameters (L and MLT), geomagnetic index (K_p), and observed electric field spectra. Their results were in good agreement with the densities obtained by AURA, and they reported the ultimate error rate of the derived density was approximately 14%, excluding cases of low density.

In recent years, deep learning (DL) has been applied to various fields, including space weather research [15]. There are various types of DL, but the core idea is to improve the ability to represent the data by deepening the layer of neural network (NN) combining simple perceptrons [16]. Convolutional neural network (CNN) is a kind of DL technique, which has a high recognition accuracy mainly in the field of image recognition. Neocognitron [17], which was conceived on the basis of neurophysiological findings in the visual cortex of the brain, is a prototype of CNNs. A CNN is fundamentally composed of convolution layers, for feature extraction, and pooling layers, which allow misalignment and are alternately arranged. CNNs have been actively studied in the field of image recognition. Many CNN models have achieved the highest recognized in recent years.

In this study, we propose an automatic determination system of UHR frequency by machine learning. Machine learning is a technique in the field of artificial intelligence to give computers the ability to learn with data. We defined the task of UHR frequency determination as a supervised regression, wherein a computer estimates UHR frequencies using a dataset comprising electric field dynamic spectra with correct UHR frequency labels. Zhelavskaya *et al.* [14] realized UHR frequency determination by simple NN, using the electric field spectra and five additional features. In contrast, we propose a more robust UHR frequency determination without using five additional features, by adopting recent CNN architectures (i.e., AlexNet, VGG16 and ResNet). In this study, we describe our machine learning approach and discuss results for the UHR frequency determination from electric field spectra observed by the PWE/HFA.

II. DATA

We used electric field power spectra (Level-2 CDF data) observed by the PWE/HFA aboard Arase, from April to December 2017, as an input for machine learning. The HFA provides wide-frequency-range (0.1–10 MHz) electric power spectra with a time resolution of 8 or 60 s. We calculated averaged (60 s resolution) power spectra when the HFA provided 8 s time resolution data. The time variation of the UHR frequencies was already determined for specific periods by a semiautomatic detection algorithm with corrections by visual inspection [8] and has been provided as Level-3 CDF data. The time resolution of the determined UHR frequency data was 60 s. We used the UHR frequency data from the Level-3 CDF data as labels for training the CNN. We used DC magnetic field data observed by the magnetic field

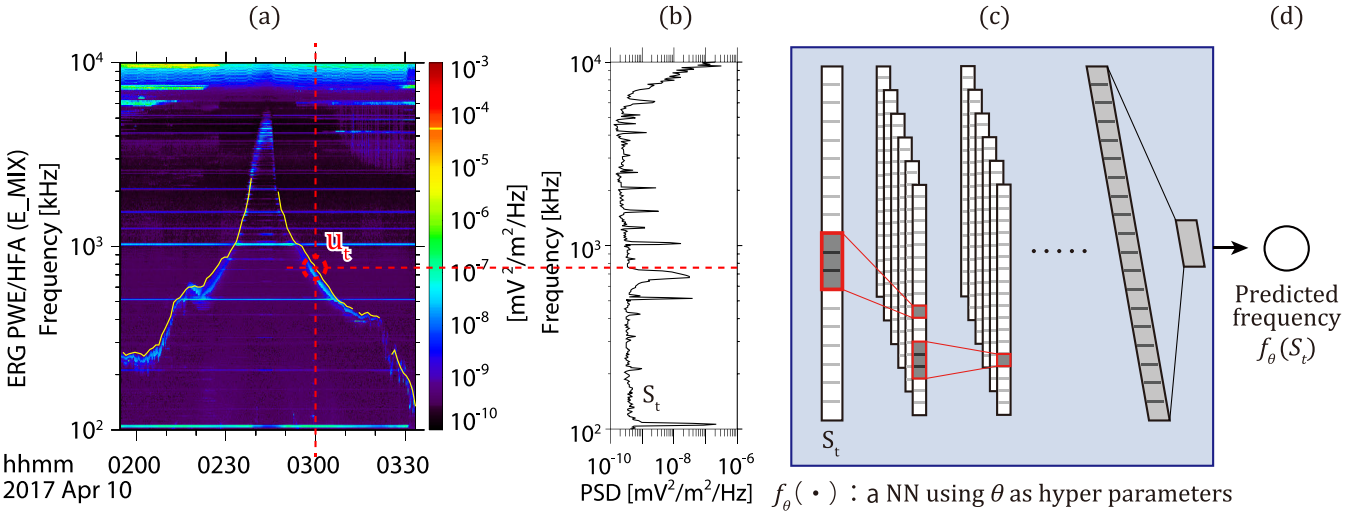

FIGURE 1. Outline of proposed method. (a) Frequency-time diagram of electric field spectra observed by high frequency analyzer (HFA) and labeled upper hybrid resonance (UHR) frequency (yellow line.) (b) Observed electric field spectrum, S_t, at time t. (c) Neural network model using S_t as an input. (d) Predicted UHR frequency.

experiment (MGF) aboard Arase [18] to calculate local electron cyclotron frequencies, f_{ce}.

Fig. 1(a) represents an example of the electric field spectra observed by the HFA on April 10, 2017. The UHR emission was observed during the period in the frequency range of 100 to 6000 kHz, depending on the variation of the electron density along the orbit. The yellow line illustrated in Fig. 1(a) represents the UHR frequency labels determined by the semiautomatic detection algorithm, with correction by visual inspection [8]. Because of a weak UHR emission, there was a dearth of UHR frequency labels at approximately 03:20 UT. The lack of labels from 02:40 to 02:50 UT resulted from the restriction of spacecraft operation. It should be noted that the horizontal bands (i.e., those at approximately 1 MHz) were caused by interference from onboard instruments.

III. METHOD

A. FORMULATION

We formulated the problem of UHR frequency determination to be solvable via machine learning. We used the observed electric field spectrum at time t as a one-dimensional vector $(S_t,)$ and the label of the UHR frequency as scalar data (u_t) (see Fig. 1(b)). This problem can be formulated as a regression problem that determines u_t from the input S_t. The loss of this optimization problem can be expressed by the following equation:

$$L_\theta = \frac{1}{T}\sum_{t=1}^{T}(u_t - f_\theta(S_t))^2, \tag{3}$$

where f_θ denotes an NN (see Fig. 1(c)) with parameter θ. $f_\theta(S_t)$ is an estimation result of this NN when the input is S_t (see Fig. 1(d)). L_θ is a function that indicates the loss when using the NN with parameter θ, and T is the number of S_t in the dataset. In this study, we use the mean square error (MSE) as the loss function, since it is commonly used for regression problems. Optimizing θ that it minimizes the loss function, L_θ leads to a high performance by the f_θ of the NN in the UHR frequency determination.

The function $f(\cdot)$, which determines the UHR frequency, can be constructed using general machine learning algorithms. Zhelavskaya *et al.* [14] defined five features adopted on the basis of expert knowledge and determined the UHR frequencies using a simple multi-layer perceptron (MLP) that used input spectra, S_t, and the additional five features. It has been noted that if raw data, such as images, are used directly as the input for machine learning, the input becomes high-dimensional and the generalization performance decreases owing to the curse of dimensionality. Therefore, as a preprocessing step, the feature representation was extracted from raw data by several algorithms on the basis of expert knowledge, and the feature representation was used for the training phase of machine learning. In a related study [14], no such feature extraction was performed, and a simple MLP had the role of extracting feature representation. However, it is likely that such a simple MLP cannot sufficiently learn feature representations.

Our proposed method improves on the following two points in relation to the method proposed in the related study [14]. First, our method does not use the features adopted in the related study on the basis of expert knowledge; we instead perform end-to-end UHR frequency determination using only the observed electric field spectra. Second, we use a CNN as a method for extracting feature representations from the observed electric field spectra. It is known that CNNs extract more advanced feature representations than does the simple MLP adopted in the related study. Furthermore, by adopting an advanced CNN architecture that has achieved a high accuracy in the field of image recognition, we can identify a suitable model for UHR

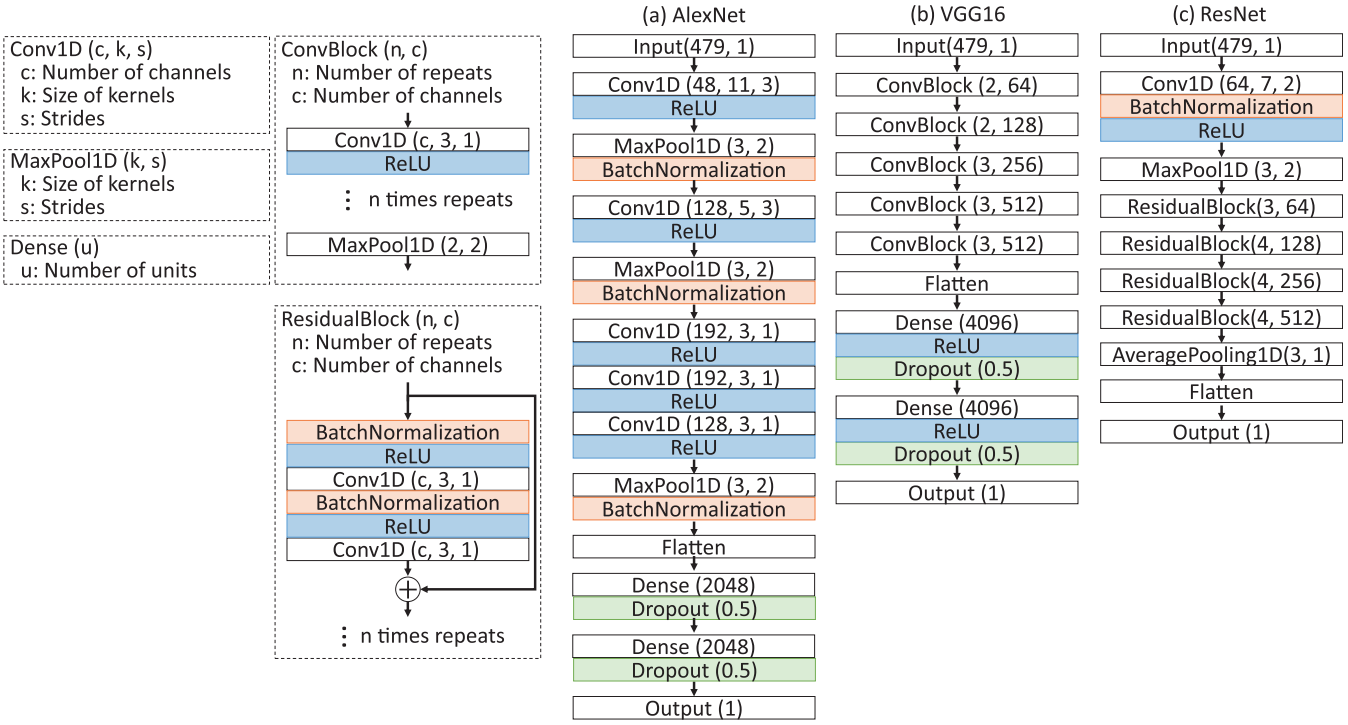

FIGURE 2. Architectures of the adopted CNN models: (a) AlexNet model, (b) VGG16 model, (c) ResNet model.

frequency determination. For simplicity, we determine UHR frequencies by using a time-independent system.

B. CONVOLUTIONAL NEURAL NETWORKS

The CNN architectures described in the next section comprise the layers described in this section.

The hidden layer used in conventional NNs is called the fully connected (FC) layer. In the lth FC layer, let the output for the next layer $\boldsymbol{h}^{(l+1)}$ be the result of a product-sum operation of all inputs $\boldsymbol{h}^{(l)}$ and the weights vector, as demonstrated by the following formula:

$$\boldsymbol{h}^{(l+1)} = g^{(l)}(\boldsymbol{W}^{(l)T}\boldsymbol{h}^{(l)} + \boldsymbol{b}^{(l)}), \tag{4}$$

where (l) is the lth layer, $g^{(l)}(\cdot)$ is the activation function, $\boldsymbol{W}^{(l)}$ is the weights vector, and $\boldsymbol{b}^{(l)}$ is the bias. A two-to three-layer model constructed with only the FC layer is generally called an MLP, whereas a deeper model is called a deep neural network. One problem with the FC layer is that the shape and order of the data are ignored. Because our input, S_t, consists of information that changes continuously in the frequency direction, the shape and order of the data may provide useful information for UHR frequency determination.

In the convolutional layer, the shape of the input is maintained by performing the operation of convoluting a kernel value to the input. The output for the next layer in the convolution layer is calculated by sliding a convolutional kernel over the inputs. For example, when the input vector and convolutional kernel are $\{1, 2, 3, 4\}$ and $\{1, 2\}$ respectively, the output vector is $\{5, 8, 11\}$. The convolutional kernel plays a role similar to that of the weights vector; however, the kernel value is shared regardless of the convolutional coordinates, and a single layer handles multiple kernel values.

A pooling layer is generally also used in the CNN. The pooling layer does not have parameters such as the weights vector that are optimized in the training phase. The input is divided by kernel size, and each representative value is calculated as an output for the following layer. For example, when the input vector is $\{1, 2, 3, 4\}$ and the kernel size is 2, then the output vector is $\{2, 4\}$ in the max pooling case.

C. CNN ARCHITECTURES

CNN architectures have been studied extensively, particularly in the field of image recognition. Because no existing models have been applied to the automatic classification of plasma waves, we selected several models that demonstrated high accuracy in image recognition. In this study, we implemented and compared three models to identify a suitable model for UHR frequency detection.

The models were AlexNet, VGG16, and ResNet, and all of them achieved a high accuracy in the ImageNet Large Scale Visual Recognition Challenge (ILSVRC), an image recognition competition. The architectures of these models are illustrated in Fig. 2.

AlexNet [19] is an image recognition model that won the ILSVRC in 2012 and facilitated the recent trend of DL. Fig. 2(a) shows a one-dimensional vector with a size of 479 elements, given as an input, S_t, in the AlexNet model. This input vector was processed using batch normalization in the five convolution layers and the three pooling layers. Finally,

the processed tensor was reshaped into a flat vector (one-dimensional vector form) in the flatten layer, and the flat vector was processed in two FC layers (dense layers), which is equivalent to a simple MLP with dropout. The AlexNet model's global feature representation is investigated in the shallow layer using a large kernel size in the first convolution layer.

VGG16 [20] is an image recognition model that won second place in the same contest in 2014 and is a famous model that exhibits a high accuracy, despite its relatively simple architecture. Fig. 2(b) shows that the VGG16 comprises five ConvBlocks and two FC layers. VGG16 uses ConvBlocks wherein convolutions are performed n times prior to pooling. Multiple convolution layers with a small kernel size can generate the same effect as a single convolution layer using a large kernel size.

ResNet [21] is an image recognition model that won the ILSVRC in 2015, and most subsequent models are based on the ResNet structure. Fig. 2(c) shows that ResNet uses ResidualBlock, which has two paths, to realize a very deep structure. In the first path, convolutions were performed two times. In the second path, the original tensor did not go through any processes, which is called a "skip connection." The NN comprising two convolution layers learns the difference between the processed tensor and the original tensor. ResNet is the first model to enable the residual block structure to learn residues from the output of the previous layer.

Our method has the advantage that CNN enables automatic feature representations from a dataset without expert knowledge. In the conventional machine learning approach, we utilized a feature vector obtained from the raw data as an input instead of the raw data themselves. Labor and knowledge were required to perform the feature extraction because the feature vector was generally designed on the basis of an expert's knowledge. In contrast, the CNN learns this feature representation automatically from the dataset alone. The CNN has the potential to reduce the expert's labor and improve the performance. The outputs of the flatten layers in Fig. 2 were equivalent to the extracted features, which are commonly called "feature maps."

Because these models are primarily used in image recognition, the input tensor has two dimensions (height and width), and each element has three channels (RGB). However, because our method handles the one-dimensional S_t as the input, we reconstructed these models for a one-dimensional, one-channel input as illustrated in Fig. 2. In the training phase, we used MSE as the loss function to train the weights vector in the CNN model. In addition, we used the Adam optimizer [22] with a learning rate $\eta = 0.001$, $\beta_1 = 0.9$ and $\beta_2 = 0.999$, as the optimization method. Each model was trained for 1000 epochs.

IV. EVALUATION

A. EXPERIMENTAL DESIGN

We evaluated our models by comparing the accuracy of UHR frequency determination using electric field spectra observed by the PWE/HFA for 9 months, as described in Section II. We reproduced the method proposed in a related study [14] (hereinafter referred to as zMLP) as a baseline for comparing the estimation accuracy with that of our proposed method. zMLP uses the following five features, which are based on expert knowledge: (1) decimal logarithm of electron cyclotron frequency ($\log_{10} f_{ce}$), (2) L-value, (3) geomagnetic activity index (K_p), (4) magnetic local time, and (5) frequency bin with the highest power spectral density from the electric field spectra ($f\,\mathrm{bin}_{\max}$).

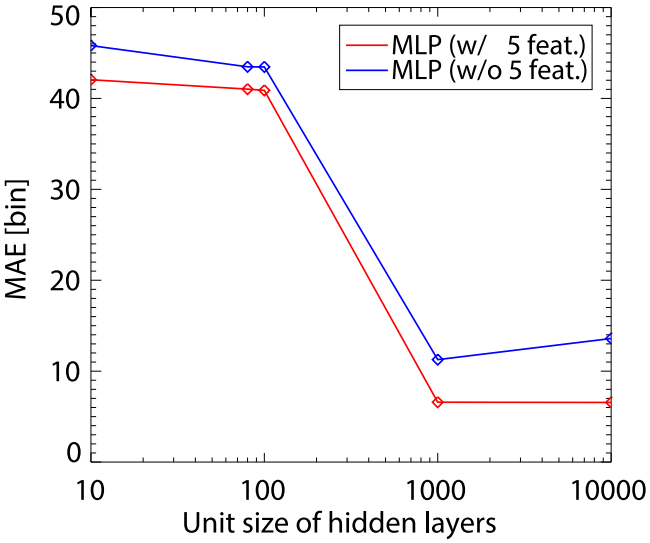

FIGURE 3. Pre-experimental results to determine the unit size of the hidden layer in the multi-layer perceptron (MLP), based on the mean absolute error (MAE).

It is common to use a 10-fold cross validation (10-fold CV) for the evaluation of a machine learning model because it minimally wastes data, which is a major advantage in cases where the number of samples is very small, such as in inverse inference. In this study, we adopted a 2-fold CV for our evaluation for the following reasons: first, we have a large amount of data (300000 records consisting of 262 days' data); second, a 10-fold CV takes too long to evaluate all models. More than a month is required to conduct a 10-fold CV for all models using a GPU (NVIDIA GeForce RTX 2080 Ti).

We used the mean absolute error (MAE) as an evaluation criterion for the model's estimation accuracy. The MAE is calculated by averaging the absolute value of the error between the correct labeling scheme and the estimated result. The HFA performs averaging among the intensities of raw spectra at neighboring frequency steps. Because the frequency resolution of observed spectra exhibits stepwise changes, as illustrated in [8], we performed the UHR frequency determination in bin units.

B. OTHER METHODS TO DETERMINE UHR FREQUENCY FOR COMPARISON

We compared six regression algorithms: elastic net, stochastic gradient descent (SGD), Bayesian ridge, support vector

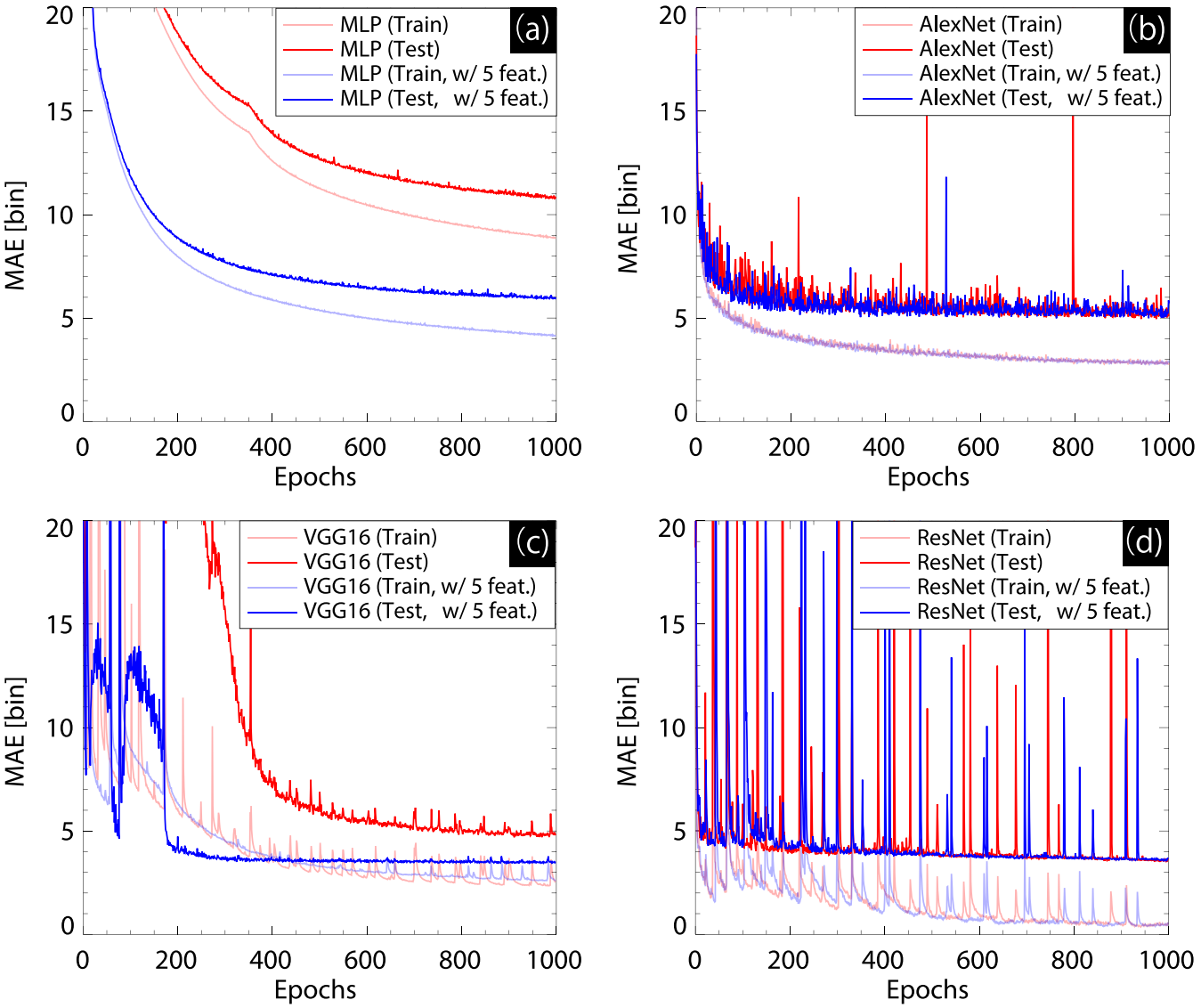

FIGURE 4. The MAEs of the derived UHR frequencies as a function of learning epoch. (a) zMLP model, (b) AlexNet model, (c) VGG16 model, (d) ResNet model.

regression (SVR) (kernerl = {linear, rbf}), and random forest in addition to the three CNN models. These algorithms were implemented in the scikit-learn package in Python 3. Elastic Net is a simple linear regression with regularization, combining the squared Euclidean (L2) norm and the absolute (L1) norm penalty, which is solved by ordinary least squares. SGD is another simple linear regression that optimizes the loss function, including the penalty (L2), optimized by stochastic gradient descent learning. Bayesian Ridge is one case of Bayesian inference for regression tasks. In Bayesian Ridge, regression coefficients are calculated as stochastic variables [23], [24]. SVR is a regression algorithm based on a support vector machine [25]. In this study, we adopted a kind of SVR algorithm called ϵ-SVR, which earned robustness on the basis of an epsilon tube. Within the epsilon tube, no penalty is associated with the training loss function with points predicted within the distance epsilon from the actual value. SVR represents non-linear functions using the kernel method functions. Therefore, we evaluated the two kernel functions: the linear kernel and the rbf (Gaussian) kernel. Random forest [26] is a type of ensemble learning, that combines tree predictors constructed using different bootstraped data samples. The regression result is equal to the average values of the predicted results by each tree. Combining many trees with different bootstrap samples improves the robustness for prediction.

C. EXPERIMENTAL RESULTS

We conducted preliminary experiments using a baseline method proposed in a related study [14]. The baseline method adopted an MLP model using electric field spectra, S_t, and five additional features as input. The number of units in the hidden layer was 80, which was determined by an

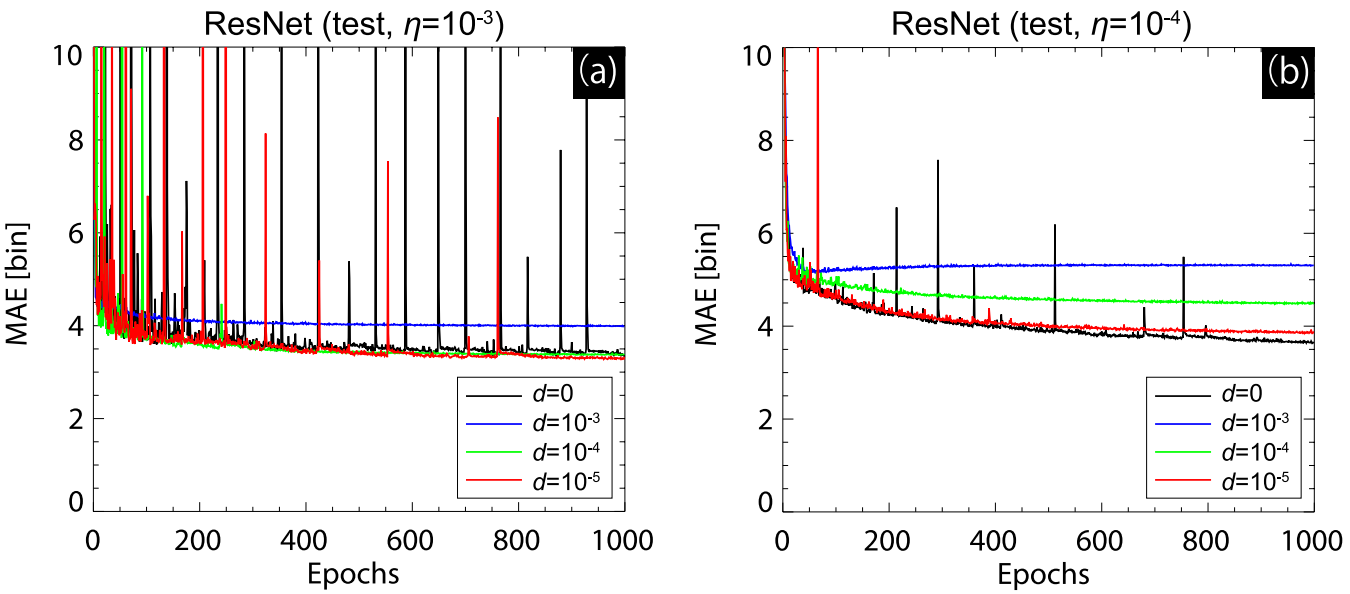

FIGURE 5. Convergence changes depending on the learning rate, η, and decay, d. The MAEs were evaluated by the ResNet model without the additional five features using single-fold dataset.

TABLE 1. The MAEs of the derived UHR frequencies according to each model, by using test data (unit: bins.).

		w/ 5 feat.	w/o 5 feat.
Conventional	zMLP	5.986	10.786
Machine learning based regression	Elastic net	64.522	68.918
	SGD	21.224	31.025
	Bayesian ridge	20.774	29.689
	SVR (linear)	21.292	32.02
	SVR (rbf)	49.27	60.486
	Random forest	4.547	6.794
This study	AlexNet	5.713	5.092
	VGG16	3.478	4.847
	ResNet	3.652	3.664

exploratory search. In the present study, we reinvestigated the appropriate unit size because the number of input dimensions greatly differed from those in the related study. Fig. 3 represents the MAE as a function of the number of units of the hidden layer in the MLP. The blue line represents the MAE when only the observed spectra, S_t, was used. In contrast, the red line represents the MAE when the additional five features were used ($\log_{10} f_{ce}$, L, K_p, MLT, and $f\,\mathrm{bin}_{max}$) together with S_t. According to the results summarized in this figure, both methods achieved good performance when the number of units was 1000; thus, we used 1000 units in our evaluation.

The first column (w/ 5 feat.) of Table 1 presents the accuracy of the UHR frequencies determined by each model when both the five features and observed electric field spectra were used. The second column (w/o 5 feat.) presents the accuracy when only the observed electric field spectra were used. When we used the five features in the CNN, we concatenated a feature map and the five features after the flatten layer, as illustrated in Fig. 2. When we used the additional five features, the VGG16 model had the smallest error (MAE = 3.478 bins), whereas the MAE of the zMLP was 5.986 bins. Of our proposed models, this one greatly improved the accuracy of UHR frequency determination in comparison with zMLP. We determined that feature representation from the observed electric field spectra was more effective using the advanced architecture of the CNNs than using the simple MLP. Our other methods using CNNs also achieved a higher accuracy (e.g., AlexNet: 5.713 and 3.652 bins) than did the zMLP model. This demonstrates that feature representation can be effectively obtained by CNNs.

When the additional five features were not used, the accuracy of the derived UHR frequencies provided by the zMLP model was approximately 80.2% lower (10.786 bins) than the accuracy with features included. In contrast, we discovered that these five features had almost no impact on the accuracy when CNN models were used. This may have resulted from the high representation ability of the ResNet model with relatively deep layers (32 layers). In addition, the feature map of the ResNet model may have acquired a representation ability comparable with five features.

Focusing on the methods using a machine-learning-based regression, only the random forest achieves a better performance than does zMLP. Although the random forest with the additional five features achieved a better performance than did the AlexNet model, it is inferior compared with the VGG16 and ResNet models irrespective of whether of the additional five features are used. The major difference between our methods and the other methods is the use of representation learning by CNN. Therefore, feature representations learned by the CNN models had a positive impact on the accuracy of determining UHR frequencies.

Thus, even though our proposed method did not use additional features based on expert knowledge, it achieved higher quality determination than did the conventional method. In particular, the ResNet model achieved a high accuracy

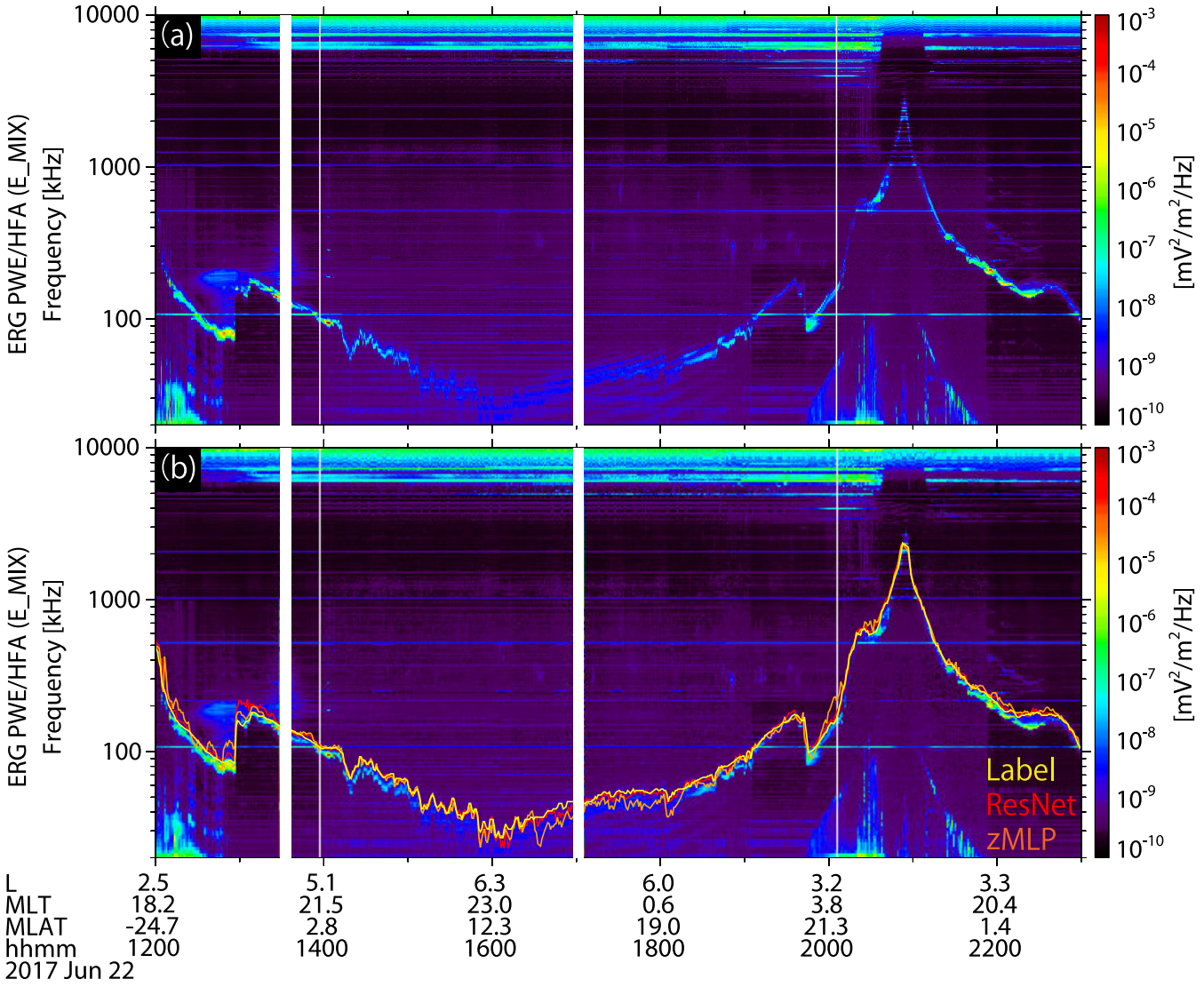

FIGURE 6. (a) Electric field spectra observed by the PWE/HFA from 12:00 to 23:00 UT, on June 22, 2017. (b) Results of the UHR frequency determination (yellow: labeled data, orange: zMLP model with the five features, red: ResNet model without the five features).

regardless of whether additional features were used. As described in the previous section, the frequency bandwidth of electric field spectra observed by the PWE/HFA changes depending on the center frequency [8]. The ResNet model achieved the highest MAE (3.664 bins) without using the additional five features. This corresponds to 4.5 kHz at the lowest frequency step (2.4–159.9 kHz) and 358.0 kHz at the highest frequency step (5.3223–10.1074 MHz).

D. CONVERGENCE OF LEARNING

Fig. 4 displays the errors of the derived UHR frequencies as a function of learning epoch. Here one epoch is defined as the time over which an entire dataset is passed both forwards and backward through the NN (only once.) The blue lines represent the MAE when the additional five features and observed electric field spectra were used, whereas the red lines represent the MAE when the additional five features are excluded. The light-colored lines represent the MAE for the training data, while the dark lines represent the MAE for the test data. As mentioned above, the accuracy of the UHR frequencies derived by the zMLP model greatly improved through the adoption of the additional five features. However, the five features were less effective for the three CNN models, regardless of the learning epochs.

In general, the accuracy in the training data increases, whereas the accuracy for the test data decreases. Upon examining the results of the AlexNet and VGG16 models, we determined that the difference in accuracy between the training and test data was relatively small, compared with the results of the ResNet model. This is because the AlexNet and VGG16 models have a limited representation ability because of their model architecture; that is, their model structures are not relatively deep. In contrast, the ResNet model achieved a high representation ability for the training data, and its MAE reached almost zero. In other words, ResNet reduced errors

for the test data using techniques to improve generalization performance.

The accuracy of the conventional method for the training data failed to converge around 500 epochs, whereas that of the ResNet model converged within almost 200 epochs. Furthermore, because the MAE of the ResNet model for the test data gradually decreased after 200 epochs, the estimation error can be further reduced by increasing the number of epochs.

According to Fig. 4, the MAE of the ResNet model sometimes yielded much worse accuracies. In an NN, the parameters of the NN are updated using the gradient of the loss function. When the gradient increases suddenly, an extreme deterioration in accuracy is observed, as shown in Fig. 4(d). This sudden increasing of the gradient is called ''gradient explosion.''

We consider the learning rate, η, and decay, d (for decreasing η depending on the learning progress) to reduce the effect of gradient explosions. Fig. 5 shows the convergence as a function of epochs under different η and d using the ResNet model. Fig. 5(a) shows the results when $\eta = 10^{-3}$, and Fig. 5(b) shows the results when $\eta = 10^{-4}$. By reducing η, the sudden deteriorations in the accuracy were suppressed. However, if we focus on $d = 0$, the MAE around 1000 epochs worsens. This is because it takes more epochs to achieve the best performance when we reduce the learning rate. Focusing on the decay d, we found that a large d hinders the learning progress. Considering the balance between the MAE and the learning speed, we concluded that the parameters $\eta = 10^{-3}$ and $d = 10^{-5}$ were better.

E. VISUALIZED RESULT

Fig. 6(a) presents the electric field spectra observed by the PWE/HFA aboard Arase from 12:00 to 23:00 UT on June 22, 2017, whereas Fig. 6(b) displays the results of the UHR frequency determination. The yellow line represents the UHR frequency labels determined by the semiautomatic detection algorithm with correction by visual inspection (provided as PWE/HFA Level-3 CDF) [8]. The orange and red lines represent the results of the UHR frequency determination using the zMLP model with the additional five features ($\log_{10} f_{ce}$, L, K_p, MLT, and $f\,\mathrm{bin}_{max}$), and the results using the ResNet models without the five features, respectively. The deviations of the determined UHR frequencies made by the ResNet model are smaller than those determined by the zMLP model, over an entire period. The errors of the UHR frequencies derived by the zMLP model are relatively high (MAE = 15.4 kHz) in the period from 15:00 UT to 19:00 UT because the observed UHR emission is weak. In contrast, the ResNet model retained a high accuracy (MAE = 13.0 kHz) although it was difficult to identify the UHR emission by visual inspection. As demonstrated by Kurth *et al.* [12], a wave spectrogram of UHR emission can be confounded by a number of factors, such as geomagnetic conditions and spacecraft location. Further scientific evaluation is required in future work to make use of a fully automatic determination system. An important nature of UHR emissions is that they do not vary discontinuously in time. In this study, we determined UHR frequencies by using a time-independent system. We may achieve high accuracy of UHR frequency determination by focusing on the nature of UHR emission.

V. CONCLUSION

In this study, we proposed an automatic system for determining UHR frequencies by DL for electric field spectra observed by the Arase satellite. We achieved end-to-end UHR frequency determination in which the end user is only required to prepare electric field spectra and several labeled UHR frequencies to train the model. The NURD algorithm proposed by Zhelavskaya *et al.* [14] used an MLP whose input was the observed electric field spectra and additional five features ($\log_{10} f_{ce}$, L, K_p, MLT, and $f\,\mathrm{bin}_{max}$). We developed a more robust UHR frequency determination system without using the five additional features, by adopting recent CNN architectures. These results indicated that the ResNet model achieved a high accuracy regardless of whether any additional features based on expert knowledge were used. This suggests that the feature map of the ResNet model acquired a representation ability beyond the five features. We will analyze the ability obtained by the CNNs by focusing on the weights and biases in an NN for future work. This study focuses on the numerical evaluation of the proposed models; however, scientific evaluation should be conducted in future work. In addition, we plan to discuss further applications of DL for other problems regarding plasma wave classification/determination based on the results of the present study.

ACKNOWLEDGMENT

Science data of the ERG (Arase) satellite were obtained from the ERG Science Center operated by ISAS/JAXA and ISEE/Nagoya University (https://ergsc.isee.nagoya-u.ac.jp/index.shtml.en). The Arase satellite data are publicly available in the ERG Science Center. The experimental data in this study is also publicly available (https://ergsc.isee.nagoya-u.ac.jp/dataset/2019.F-1001.shtml.en). In the present study, we use level 2 HFA v01.01 data, level 3 HFA v00.02 data and level 2 MGF v01.01 8 s data. Part of this work was done at the ERG-Science Center operated by ISAS/JAXA and ISEE/Nagoya University.

REFERENCES

[1] D. L. Carpenter, ''Whistler evidence of a 'knee' in the magnetospheric ionization density profile,'' *J. Geophys. Res.*, vol. 68, no. 6, pp. 1675–1682, Mar. 1963, doi: 10.1029/JZ068i006p01675.

[2] D. L. Carpenter, ''Whistler studies of the plasmapause in the magnetosphere: 1. Temporal variations in the position of the knee and some evidence on plasma motions near the knee,'' *J. Geophys. Res.*, vol. 71, no. 3, pp. 693–709, Feb. 1966, doi: 10.1029/jz071i003p00693.

[3] D. L. Carpenter and R. R. Anderson, ''An ISEE/whistler model of equatorial electron density in the magnetosphere,'' *J. Geophys. Res.*, vol. 97, no. 2, pp. 1097–1108, Feb. 1992, doi: 10.1029/91JA01548.

[4] J. U. Kozyra, T. E. Cravens, A. F. Nagy, E. G. Fontheim, and R. S. B. Ong, "Effects of energetic heavy ions on electromagnetic ion cyclotron wave generation in the plasmapause region," *J. Geophys. Res.*, vol. 89, no. 4, pp. 2217–2233, Apr. 1984, doi: 10.1029/JA089iA04p02217.

[5] R. Gendrin, "Waves and wave-particle interactions in the magnetosphere: A review," *Space Sci. Rev.*, vol. 18, pp. 145–200, Nov. 1975, doi: 10.1007/BF00172533.

[6] Y. Miyoshi, A. Morioka, H. Misawa, T. Obara, T. Nagai, and Y. Kasahara, "Rebuilding process of the outer radiation belt during the 3 November 1993 magnetic storm: NOAA and Exos-D observations," *J. Geophys. Res.*, vol. 108, no. 1, pp. SMP 3-1–SMP 3-15, Jan. 2003, doi: 10.1029/2001JA007542.

[7] Y. Kasahara, Y. Kasaba, H. Kojima, S. Yagitani, K. Ishisaka, A. Kumamoto, F. Tsuchiya, M. Ozaki, S. Matsuda, T. Imachi, Y. Miyoshi, M. Hikishima, Y. Katoh, M. Ota, M. Shoji, A. Matsuoka, and I. Shinohara, "The plasma wave experiment (PWE) on board the Arase (ERG) satellite," *Earth, Planets Space*, vol. 70, May 2018, Art. no. 86, doi: 10.1186/s40623-018-0842-4.

[8] A. Kumamoto, F. Tsuchiya, Y. Kasahara, Y. Kasaba, H. Kojima, S. Yagitani, K. Ishisaka, T. Imachi, M. Ozaki, S. Matsuda, M. Shoji, A. Matsuoka, Y. Katoh, Y. Miyoshi, and T. Obara, "High frequency analyzer (HFA) of plasma wave experiment (PWE) onboard the Arase spacecraft," *Earth, Planets Space*, vol. 70, May 2018, Art. no. 82, doi: 10.1186/s40623-018-0854-0.

[9] Y. Miyoshi, I. Shinohara, T. Takashima, K. Asamura, N. Higashio, T. Mitani, S. Kasahara, S. Yokota, Y. Kazama, S.-Y. Wang, P. Ho, Y. Kasahara, Y. Kasaba, S. Yagitani, A. Matsuoka, H. Kojima, Y. Katoh, K. Shiokawa, and K. Seki, "Geospace exploration project ERG," *Earth, Planets Space*, vol. 70. Dec. 2018, Art. no. 101, doi: 10.1186/s40623-018-0862-0.

[10] A. Shinbori, Y. Otsuka, T. Tsugawa, M. Nishioka, A. Kumamoto, F. Tsuchiya, S. Matsuda, Y. Kasahara, A. Matsuoka, J. M. Ruohoniemi, S. G. Shepherd, and N. Nishitani, "Temporal and spatial variations of storm time midlatitude ionospheric trough based on global GNSS-TEC and Arase satellite observations," *Geophys. Res. Lett.*, vol. 45, pp. 7362–7370, Aug. 2018, doi: 10.1029/2018GL078723.

[11] D. V. Kotov, P. G. Richards, V. Truklik, O. V. Bogomaz, M. O. Shulha, N. Maruyama, M. Hairston, Y. Miyoshi, Y. Kasahara, A. Kumamoto, F. Tsuchiya, A. Matsuoka, I. Shinohara, M. Hernandez-Pajares, I. F. Domnin, T. G. Zhivolup, L. Y. Emelyanov, and Y. M. Chepurnyy, "Coincident observations by the Kharkiv IS radar and ionosonde, DMSP and Arase (ERG) satellites, and FLIP model simulations: Implications for the NRLMSISE-00 hydrogen density, plasmasphere, and ionosphere," *Geophys. Res. Lett.*, vol. 45, pp. 8062–8071, Aug. 2018, doi: 10.1029/2018GL079206.

[12] W. S. Kurth, S. De Pascuale, J. B. Faden, C. A. Kletzing, G. B. Hospodarsky, S. Thaller, and J. R. Wygant, "Electron densities inferred from plasma wave spectra obtained by the waves instrument on Van Allen Probes," *J. Geophys. Res. Space Phys.*, vol. 120, pp. 904–914, Oct. 2015, doi: 10.1002/2014JA020857.

[13] B. H. Mauk, N. J. Fox, S. G. Kanekal, R. L. Kessel, D. G. Sibeck, and A. Ukhorskiy, "Science objectives and rationale for the radiation belt storm probes mission," *Space Sci. Rev.*, vol. 179, nos. 1–4, pp. 3–27, Nov. 2012, doi: 10.1007/s11214-012-9908-y.

[14] I. S. Zhelavskaya, M. Spasojevic, Y. Y. Shprits, and W. S. Kurth, "Automated determination of electron density from electric field measurements on the Van Allen Probes spacecraft," *J. Geophys. Res. Space Phys.*, vol. 121, pp. 4611–4625, May 2016, doi: 10.1002/2015JA022132.

[15] E. Camporeale, "The challenge of machine learning in space weather: Nowcasting and forecasting," *Space Weather*, vol. 17, pp. 1166–1207, Aug. 2019, doi: 10.1029/2018SW002061.

[16] F. Rosenblatt, "The perceptron: A probabilistic model for information storage and organization in the brain," *Psychol. Rev.*, vol. 65, no. 6, pp. 386–408, Dec. 1958.

[17] K. Fukushima and S. Miyake, "Neocognitron: A new algorithm for pattern recognition tolerant of deformations and shifts in position," *Pattern Recognit.*, vol. 15, no. 6, pp. 455–469, Dec. 1982.

[18] A. Matsuoka, M. Teramoto, R. Nomura, M. Nose, A. Fujimoto, Y. Tanaka, M. Shinohara, T. Nagatsuma, K. Shiokawa, Y. Obana, Y. Miyoshi, M. Mita, T. Takashima, and I. Shinohara, "The ARASE (ERG) magnetic field investigation," *Earth, Planets Space*, vol. 70, Mar. 2018, Mar. 2018, doi: 10.1186/s40623-018-0800-1.

[19] A. Krizhevsky, I. Sutskever, and G. Hinton, "ImageNet classification with deep convolutional neural networks," in *Proc. 25th Int. Conf. Neural Inf. Process. Syst. (NIPS)*, vol. 1, Dec. 2012, pp. 1097–1105.

[20] K. Simonyan and A. Zisserman, "Very deep convolutional networks for large-scale image recognition," in *Proc. Int. Conf. Learn. Represent.*, May 2015, pp. 1–14.

[21] K. He, X. Zhang, S. Ren, and J. Sun, "Deep residual learning for image recognition," in *Proc. IEEE Conf. Comput. Vis. Pattern Recognit. (CVPR)*, Jun. 2016, pp. 770–778, doi: 10.1109/CVPR.2016.90.

[22] D. P. Kingma and J. L. Ba, "Adam: A method for stochastic optimization," in *Proc. Int. Conf. Learn. Represent.*, May 2015, pp. 1–13.

[23] D. J. C. MacKay, "Bayesian interpolation," *Neural Comput.*, vol. 4, no. 3, pp. 415–447, 1992, doi: 10.1162/neco.1992.4.3.415.

[24] M. E. Tipping, "Sparse Bayesian learning and the relevance vector machine," *J. Mach. Learn. Res.*, vol. 1, pp. 211–244, Sep. 2001.

[25] C. C. Chang and C. J. Lin, "LIBSVM: A library for support vector machines," *ACM Trans. Intell. Syst. Technol.*, vol. 2, no. 3, pp. 1–27, 2011, doi: 10.1145/1961189.1961199.

[26] L. Breiman, "Random forests," *Mach. Learn.*, vol. 45, no. 1, pp. 5–32, 2001, doi: 10.1023/A:1010933404324.

TATSUHITO HASEGAWA (M'13) received the Ph.D. degree in engineering from Kanazawa University, in 2015. From 2011 to 2013, he was a System Engineer with Fujitsu Hokuriku Systems Ltd. From 2014 to 2017, he was an Assistant with Tokyo Healthcare University. Since 2017, he has been a Senior Lecturer with the Graduate School of Engineering, University of Fukui. His research interests include human activity recognition, applying deep learning, and intelligent learning support systems. He is a member of IPSJ, HIS, and JASAG.

SHOYA MATSUDA received the Ph.D. degree in engineering from Kanazawa University, in 2015. He was a Research Fellow for Young Scientists of JSPS, from 2014 to 2018. Since 2018, he has been an Aerospace Project Research Associate with the Institute of Space and Astronautical Science (ISAS)/Japan Aerospace Exploration Agency (JAXA). He is a member of SGEPSS, JpGU, AOGS, and AGU.

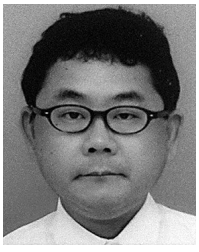

ATSUSHI KUMAMOTO received the B.S., M.S., and Ph.D. degrees in geophysics from Tohoku University. From 1998 to 2008, he was an Assistant Professor with the Department of Geophysics, Tohoku University, where he has been an Associate Professor, since 2008. He was a Co-Investigator of plasma wave receivers onboard Japanese Scientific Spacecrafts, such as Akebono (Auroral Explorer), Kaguya (Lunar Orbiter), and Arase (Geospace Explorer), and a Principal-Investigator of plasma wave receivers and impedance probes onboard the sounding rockets for observation of the ionosphere. His research interests include planetary plasma physics and planetary subsurface radar sounding.

FUMINORI TSUCHIYA received the Ph.D. degree in science from Tohoku University, in 2009. He has been a Research Associate with the Graduate School of Science, Tohoku University. He is a member of SGEPSS, JpGU, DPS/AAS, and AGU.

YOSHIYA KASAHARA received the Ph.D. degree in the field of electrical engineering from Kyoto University, in 1996. He had been a Research Associate with Kyoto University, since 1992. He joined Kanazawa University, as an Associate Professor, in 2002. He is currently a Professor with Kanazawa University, and also a Visiting Professor with Nagoya University. His research interests include radio science, intelligent signal processing, theoretical studies on generation, and propagation mechanism of waves in space plasma. He is a member of SGEPSS, JpGU, IEICE, IPSJ, AGU, and AOGS.

YOSHIZUMI MIYOSHI (M'16) received the Ph.D. degree in science from Tohoku University, Sendai, in 2001. He has been a Professor with the Institute for Space-Earth Environmental Research and the Graduate School of Engineering, Nagoya University, since 2018. He is also a Project Scientist of the ERG (Arase) Project and a Manager of the ERG Science Center. He is a member of SICE, JSME, SGEPSS, JpGU, AOGS, and AGU.

YASUMASA KASABA received the Ph.D. degree in engineering from Kyoto University, Kyoto, in 1997. He was a Research Associate with Toyama Prefectural University and an Associate Professor with the Institute of Space and Astronautical Science (ISAS)/Japan Aerospace Exploration Agency (JAXA). He is currently a Professor and the Director of the Planetary Plasma and Atmospheric Research Center (PPARC), Tohoku University. He is a member of AGU, ASJ, JpGU, JSPS, and SGEPSS.

AYAKO MATSUOKA received the Ph.D. degree in science from The University of Tokyo, in 1994. Since 1994, she had been a Research Associate with the Institute of Space and Astronautical Science (ISAS), reorganized into Japan Aerospace Exploration Agency (JAXA), in 2003, where she has also been an Associate Professor, since 2005. She has studied the magnetic fields measured by satellites in space and the physics of the magnetohydrodynamic waves. She has participated in the Japanese and international spacecraft missions exploring the terrestrial magnetosphere and planetary environment. She is a member of SGEPSS, JpGU, AGU, and AOGS.

IKU SHINOHARA received the Ph.D. degree in science from The University of Tokyo, in 1997. He was a Research Associate with the Institute of Space and Astronautical Science. He is currently an Associate Professor and a Project Manager of the ERG (Arase) Project with the Institute of Space and Astronautical Science/Japan Aerospace Exploration Agency. He is a member of SGEPSS, JpGU, EGU, and AGU.